

Exciton condensation in biased bilayer graphene

Harley D. Scammell¹ and Oleg P. Sushkov¹

¹*School of Physics, the University of New South Wales, Sydney, NSW, 2052, Australia*

(Dated: January 20, 2023)

We consider suspended bilayer graphene under applied perpendicular electric bias field that is known to generate a single particle gap 2Δ and a related electric polarization \mathcal{P} . We argue that the bias also drives a quantum phase transition from band insulator to superfluid exciton condensate. The transition occurs when the exciton binding energy exceeds the band gap 2Δ . We predict the critical bias (converted to band gap), $\Delta_c \approx 60$ meV, below which the excitons condense. The critical temperature, $T_c(\Delta)$, is maximum at $\Delta \approx 25$ meV, $T_c^{\max} \approx 115$ K, decreasing significantly at smaller Δ due to thermal screening. Entering the condensate phase, the superfluid transition is accompanied by a cusp in the electric polarization $\mathcal{P}(\Delta)$ at $\Delta \rightarrow \Delta_c$, which provides a striking testable signature. Additionally, we find that the condensate prefers to form a pair density wave.

Introduction — Excitonic condensates in two-dimensional (2D) materials promise novel superfluid [1–5] or topological [6–11] properties, and have thereby attracted considerable theoretical and experimental attention. Moreover, due to these novel transport behaviours, excitonic condensates promise a route to future technological advancements. So far, however, experimental realisations of the desired condensate have proven problematic.

Theoretically it is convenient to classify exciton condensates (also known as exciton insulators) by the nature of the corresponding interaction-driven quantum phase transition. *Class I* corresponds to the (semi)metal-to-exciton condensate phase transition [12–14]. In this case there are simultaneous Fermi surfaces of electrons and holes. If the Fermi surfaces are identical, an arbitrarily weak attraction between electrons and holes leads to condensation. This situation is analogous to BCS superconductivity. *Class II* corresponds to the band insulator-to-exciton condensate phase transition. In this case there is no Fermi surface and the interaction must exceed a critical value to generate the condensate.

Graphene layers, with their very near particle-hole symmetry, have provided a hunting ground for exciton condensation. Previous theoretical considerations include bilayer graphene (BLG) — unbiased with AB stacking [15–17] or biased with AA stacking [18, 19]. There have been no corresponding experimental detections of condensation.

Another set of proposals are graphene double layers [20–24] or double bilayers [25–28], separated by a dielectric. Theoretical predictions for the Berezinskii–Kosterlitz–Thouless (BKT) transition temperature for such systems vary significantly from room temperature in Ref. [20] to 1 mK in Refs. [23, 24] — the key difference arises due to the inclusion [23, 24] or exclusion [20] of Coulomb screening. Experimentally, there is one recent indirect indication of possible zero-magnetic field exciton condensation in double-bilayer graphene with WSe₂ spacer [29] and also in an InAs/GaSb bilayer [30], with both scenarios belonging to Class I. On the other hand, there have been several experimental reports of exciton condensation in quantum Hall regime in strong

magnetic field for double-layer graphene [31–33] or other double layer systems [34–36]; such excitonic pairing occurs between different Landau levels.

Most, if not all, previous studies of exciton condensation have been aimed at class I. However, class I is necessarily a many-body problem and progress often requires uncontrolled approximations. Here, instead, we consider condensation in class II. A striking technical advantage is that we only need to consider a two-body problem. In class II the condition of exciton condensation is the equality of the exciton binding energy ϵ_b to the single particle band gap, 2Δ . The present work is focused on biased BLG. Unbiased BLG is a semimetal, however, application of an electric bias (perpendicular electric field) opens a single particle band gap 2Δ [37] — placing it within class II. The bias is created by symmetric metallic gates above and below the plane.

A careful treatment of the screened attractive electron-hole Coulomb interaction is essential to make quantitative predictions of the binding energy and hence of the condensation transition. To this end, we account for three sources of screening: (i) Screening by metallic gates placed a distance d above and below the BLG plane; (ii) dielectric screening due to a material between BLG and the gates; and (iii) BLG self-screening and retardation thereof, as captured via the Random Phase Approximation (RPA). We find that all three sources of screening significantly influence, i.e. reduce, the condensation critical temperature. To this end, we propose idealised experimental setups to allow to maximise the critical temperature. A key development in this work is our treatment of the retardation of the self-screening, i.e. retardation of the screened Coulomb potential.

The key development of this work is that we are able to: use reliable two-body techniques to describe excitonic bound states in a band insulator; account for environmental sources of screening; treat dynamically screening/retardation. This combination affords a reliable prediction of the critical temperature, and how it may be optimised with respect to system parameters. Entering the exciton condensate phase, we lose this quantitative control over the problem, and instead resort to mean-

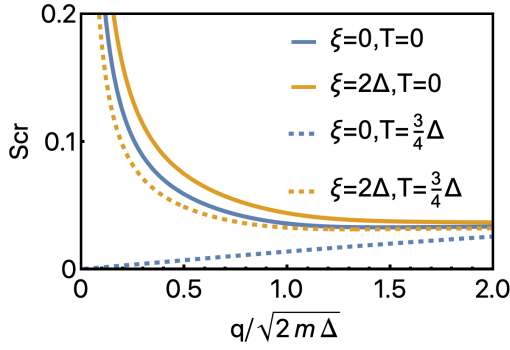


FIG. 1. Screening factor vs momentum for $\Delta = 10\text{meV}$, $d=1000\text{nm}$, $\epsilon_r = 1$. The factor is presented for two imaginary frequencies, $\xi = 0$, $\xi = 2\Delta$, and for two temperatures, $T = 0$, $T = 3\Delta/4 = 87\text{K}$.

field theory. We note that the exciton condensate is a neutral superfluid, and that experimentally distinguishing between this and the band insulator phase is subtle. Using our mean-field description, we establish two key experimental signatures of the excitonic condensate.

Methods — We consider biased bilayer graphene for which the low-energy single particle Hamiltonian can be reduced to [38]

$$H_0 = \begin{pmatrix} \Delta - \mu & -\frac{p_x^2}{2m} \\ -\frac{p_x^2}{2m} & -\Delta - \mu \end{pmatrix}. \quad (1)$$

H_0 is written in terms of $\{A_1, B_2\}$ orbitals, with A, B referring to graphene sublattice and subscripts 1, 2 referring to layers. Here $p_{\pm} = \tau p_x \pm ip_y$, \mathbf{p} is the in-plane momentum, $\tau = \pm 1$ the valley quantum number, $m \approx 0.032m_e$ the effective mass, and Δ is proportional to the bias electric field, $\Delta \propto E$, [39]. The chemical potential μ is set to zero (half-filling) for the rest of this work. There are corrections to (1) related to electron-hole asymmetry, trigonal warping, etc. However, influence of all these corrections on the exciton is negligible at $\Delta < 60\text{meV}$, see Ref.[40], so here we disregard the corrections. Hence electron and hole dispersions, denoted $\omega_{\mathbf{p}}^{(\pm)}$, are symmetric about $\mu = 0$, i.e. $\omega_{\mathbf{p}}^{(\pm)} = \pm\omega_{\mathbf{p}}$, with $\omega_{\mathbf{p}} = \sqrt{\Delta^2 + p^4/(4m^2)}$. Application of the bias induces electric polarisation along the field. If $a \approx 0.3\text{nm}$ is the separation between the planes and e is the electron charge, the electric dipole moment per unit area is $|e|a\mathcal{P}_{\Delta}$, with the layer polarization \mathcal{P}_{Δ} , due to the bias $\propto \Delta$, given by

$$\mathcal{P}_{\Delta} = 4 \int \frac{d^2p}{(2\pi)^2} (|\beta_{\mathbf{p}}^{(-)}|^2 - |\alpha_{\mathbf{p}}^{(-)}|) = \frac{2m\Delta}{\pi} \ln \frac{\Lambda}{|\Delta|}. \quad (2)$$

The factor 4 is due to the spin and valley degeneracy, $\alpha_{\mathbf{p},\tau}^{(-)}$ and $\beta_{\mathbf{p},\tau}^{(-)}$ are upper and lower components of the negative energy eigenfunction (for a given valley), and Λ is the ultraviolet energy cutoff. We confirm via a direct calculation that including the next two orbitals, i.e. $\{A_2, B_1\}$, naturally cuts off of the UV divergence;

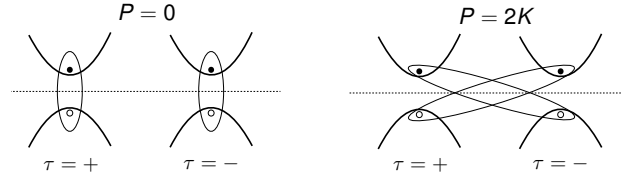


FIG. 2. Inter- and intra-valley excitons: intravalley have zero total momentum $\mathbf{P} = \mathbf{0}$, while intervalley have $\mathbf{P} = 2\mathbf{K}$, with \mathbf{K} the valley momentum.

the choice $\Lambda = 0.5\text{eV}$ in (2) is consistent with the direct four-orbital calculation.

Attraction between electron and hole is due to the screened Coulomb interaction

$$V_{\mathbf{q},i\xi} = -\frac{2\pi e^2}{\epsilon_r q / \Upsilon_q - 2\pi e^2 \Pi(\mathbf{q}, i\xi, T)} \quad (3)$$

Here \mathbf{q} is the momentum transfer, ξ is the imaginary frequency transfer, and T is temperature. Other parameters are: (i) $\Upsilon_p = \tanh(pd)$ accounts for the metallic gate screening, at a distance d above and below the BLG plane; (ii) ϵ_r is the dielectric constant of the substrate/superstrate material between BLG and gates; and (iii) $\Pi(\mathbf{q}, i\xi, T)$ is the polarisation operator of BLG, with details presented in the Supplement [41]. To demonstrate key features of (3), we introduce a screening factor – defined as the ratio of the screened interaction (3) to the bare Coulomb interaction, $-2\pi e^2/(\epsilon_r q)$. The screening factor provides a measure of the effectiveness of screening. Fig. 1 demonstrates that the screening very strongly depends on frequency and on temperature. Notably, thermally excited electrons practically fully screen the static interaction, i.e. the screening factor becomes vanishingly small.

A frequency dependence of $V_{\mathbf{q},i\xi}$ corresponds to retardation of the interaction in the time-domain. For a weakly-bound exciton in an insulator, with binding energy $\epsilon_b \ll 2\Delta$, retardation is not important [40]. However, retardation becomes essential for strongly-bound excitons $\epsilon_b \sim 2\Delta$. We point out that the condition for exciton condensation, $\epsilon_b = 2\Delta$, necessarily implies strongly-bound excitons and therefore retardation is important. To properly treat retardation in the exciton binding problem, one has to employ the Bethe-Salpeter equation (BSE) [42]

$$\chi_{\xi_n, \mathbf{k}} = -T \sum_m \int \frac{d^2k'}{(2\pi)^2} \frac{V_{\mathbf{k}-\mathbf{k}', i(\xi_n - \xi_m)} Z_{\mathbf{k}, \mathbf{k}'}^{\tau', \tau}}{(E/2 - \omega_{\mathbf{k}})^2 + \xi_n^2} \chi_{\xi_m, \mathbf{k}'}, \quad (4)$$

written in terms of the amputated two-particle Green's function $\chi_{\xi_n, \mathbf{k}}$. Here $E = 2\Delta - \epsilon_b$, $\xi_n = (2n + 1)\pi T$ and $Z_{\mathbf{k}, \mathbf{k}'}^{\tau', \tau} = \langle \psi_{\mathbf{k}, \tau'}^{(-)} | \psi_{\mathbf{k}', \tau'}^{(-)} \rangle \langle \psi_{\mathbf{k}', \tau}^{(+)} | \psi_{\mathbf{k}, \tau}^{(+)} \rangle$ is the vertex form factor, with $\psi_{\mathbf{k}, \tau}^{(\pm)}$ denoting the single particle wavefunctions for conduction and valence bands of (1), see also [41]. The total momentum of the electron and hole is encoded in the valley indices, and is either zero for $\tau = \tau'$ (intravalley pairing) or non-zero for $\tau = -\tau'$ (intervalley

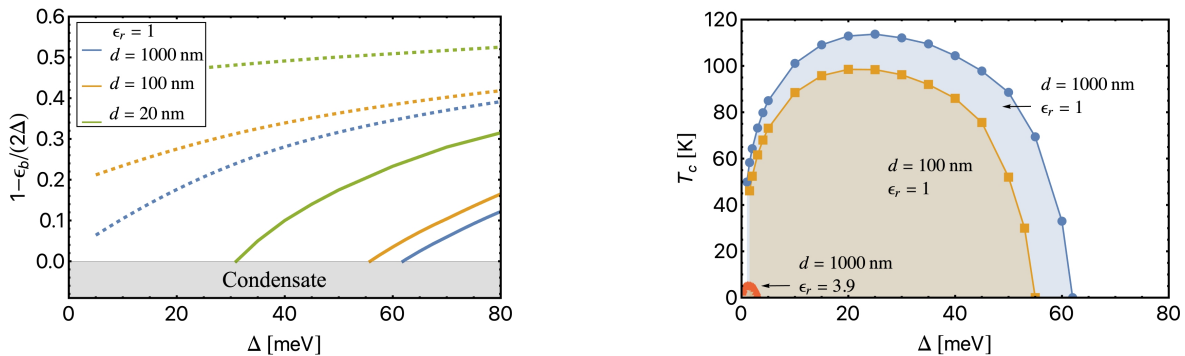


FIG. 3. (a) Exciton binding energy at $T = 0$ and three values of distance to gates, $d = 20, 100, 1000$ nm vs the band gap, at $\epsilon_r = 1$. Dashed lines correspond to LSE and solid lines to BSE. (b) Superfluid domes, for the following sets of parameters: $\{\epsilon_r = 1, d = 1000\text{nm}\}$, $\{\epsilon_r = 1, d = 100\text{nm}\}$, $\{\epsilon_r = 3.9, d = 1000\text{nm}\}$. Points represent T_c versus the band gap parameter Δ , as computed from the BSE (4).

pairing) – as depicted in Fig. 2. The form factors do not distinguish spin, yet they weakly distinguish between intra- and intervalley pairing; the implications for the condensate phase is discussed later. The interaction has an $SU(2) \times SU(2)$ spin-symmetry – correspondingly, the exciton bound state has an $SO(4)$ spin symmetry relating the spin-singlet and triplet configurations.

We pause to mention that under an instantaneous interaction, $V_{\mathbf{k}-\mathbf{k}'}$, e.g. as obtained by ignoring the frequency dependence of screening, the exciton can be described by a wave function that obeys the Lippmann-Schwinger equation (LSE),

$$(E_0 - 2\omega_{\mathbf{k}})\Psi_{\mathbf{k}} = \int \frac{d^2k'}{(2\pi)^2} V_{\mathbf{k}-\mathbf{k}'} Z_{\mathbf{k},\mathbf{k}'}^{\tau',\tau} \tanh\left(\frac{\omega_{\mathbf{k}'}}{2T}\right) \Psi_{\mathbf{k}'}. \quad (5)$$

LSE is a linear eigenvalue problem and can be easily solved to find the eigenenergy E_0 and eigenfunction $\Psi_{\mathbf{k}}$; solution of (5) shows that the Lippmann-Schwinger wave function $\Psi_{\mathbf{k}}$ is well localised in the momentum space, $k \lesssim \sqrt{2m\Delta}$. This corresponds to the exciton spatial size $r \sim 1/\sqrt{2m\Delta}$. We see a hint that the wavefunction approach is problematic at $\Delta \rightarrow 0$. We denote the binding energy computed from LSE as $\epsilon_b^0 = 2\Delta - E_0$.

Phase diagram – Via direct computation of Eq. (4), the intervalley s -wave exciton is found to have the lowest energy for $\Delta > 0$; we henceforth specialise to this state. Let us start from $T=0$. Fig. 3a shows the exciton binding energy vs the gap parameter Δ for $\epsilon_r = 1$ and three values of distance to the gate $d = \{20, 100, 1000\}$ nm; the solid and dashed lines are computed from the BSE (4) and LSE (5), respectively, whereby only the BSE includes retardation effects. First, we see that retardation significantly influences the binding energy — one could think of retardation of the screened potential acting as an effective dynamic boson mode which is enhancing the binding of electrons and holes. Second, the plot marks a condensation region, whereby $\epsilon_b \geq 2\Delta$. At $\epsilon_r = 1$, condensation occurs for gates placed beyond a critical distance $d > d_c \approx 10 - 15$ nm. In particular, for

$d = \{20, 100, 1000\}$ nm the quantum critical point is $\Delta_c = \{31, 55, 62\}$ meV. Considering instead hBN encapsulation, such that $\epsilon_r = 3.9$, and taking $d = 100$ nm, the critical point is reduced to $\Delta_c = 3$ meV. These results highlight the strong influence of gate and dielectric screening on the excitonic binding energy and condensation transition.

To establish the phase boundary of Fig. 3(b), we solve $\epsilon_b(T_c) = 2\Delta$. We note that for $\Delta < \Delta_c$, the two-particle problem makes sense only at or above the critical temperature, where T_c is understood to be a BKT transition temperature. For $\epsilon_r = 1$ and $d = \{100, 1000\}$ nm maximum critical temperatures are significant, $T_c \approx \{100, 115\}$ K, respectively. For $\epsilon_r = 3.9, d = 100$ nm the superfluid dome is comparatively small. Fig. 3(b) shows that as $\Delta \rightarrow 0$, the $T_c(\Delta)$ is rapidly decreasing. However, we stress that we do not propagate the BSE technique down to exactly $\Delta = 0$; here the system becomes semi-metallic and the two-body technique employed here becomes prohibitively expensive numerically. Physically, the strong suppression of T_c at small band gap Δ is due to the enhanced thermal excitation to the conduction band; the thermally excited states act as a source of metallic screening, and thereby have a significant affect on the Coulomb attraction. This feature, i.e. strongly enhanced screening, makes this problem highly non-BCS; BCS provides a simple relation between $T = 0$ order parameter and T_c , which derives from the Pauli blocking factor (i.e. thermal occupation factors). In our case, we have both (thermal) Pauli blocking as well as thermal screening of the interaction. We find that the thermal screening plays the dominant role in melting the order, and thus we do not recover the standard BCS relation.

Finally, we mention that within the BSE two-body formalism we arrive at the following critical scaling of T_c near $\Delta \rightarrow \Delta_c^-$ (see Supplement [41]),

$$T_c(\Delta) \sim \Delta_c / \ln\left(\frac{g\Delta_c}{\Delta_c - \Delta}\right) \quad (6)$$

where g is a dimensionless combination of the interaction strength and density of states, as well as other dimension-

less numerical factors that we do not evaluate.

Condensate phase — Entering the condensate phase we can no longer apply two-body techniques, and therefore do not expect to make quantitative predictions. Even so, the results below provide crucial predictions for future experimental tests of the exciton condensate. The discussion from here on will be based on a mean-field Hamiltonian, $H_{\text{MF}} = \sum_{\mathbf{p},\tau,s} c_{\mathbf{p},\tau,s}^\dagger \omega_{\mathbf{p}} c_{\mathbf{p},\tau,s} + v_{\mathbf{p},\tau,s}^\dagger (-\omega_{\mathbf{p}}) v_{\mathbf{p},\tau,s} + \sum_{\mathbf{p},\tau,\tau',s,s'} c_{\mathbf{p},\tau,s}^\dagger \Phi(p)_{\tau,\tau,s,s'} v_{\mathbf{p},\tau',s'} + \text{h.c.}$, with $c_{\mathbf{p},\tau,s}^\dagger (v_{\mathbf{p},\tau,s}^\dagger)$ the creation operators for conduction (valence) electrons, and with $\Phi(p)_{\tau,\tau,s,s'}$ the order parameter. Explicitly for the s -wave intervalley excitonic condensate, it takes the form

$$\Phi(p)_{\tau,\tau',s,s'} = \Phi_0(p) (\tau_x)_{\tau,\tau'} e^{i\frac{(\tau-\tau')}{2}\phi} (d_\mu s_\mu i s_y)_{s,s'}, \quad (7)$$

where $\Phi_0(p)$ is the amplitude; ϕ an arbitrary phase encoding the phase difference between the two distinct intervalley states, i.e. those with valley indices $(\tau, \tau') = (+-)$ and $(-+)$; τ_x is a Pauli matrix acting on valley indices; s_μ are Pauli spin matrices and d_μ are the components of a unit four-vector, with $\mu = 0$ corresponding to a spin-singlet and $\mu = 1, 2, 3$ to the components of the spin-triplet — there is an SO(4) degeneracy of this spin ordering vector (d_μ).

We pause to note that a spontaneous symmetry breaking in *unbiased* bilayer graphene has been considered [15]. Specifically, that work predicts a spontaneous ferroelectric polarisation perpendicular to the plane, breaking a \mathbb{Z}_2 ‘layer’ symmetry. By contrast, in the present work the applied electric bias explicitly breaks the \mathbb{Z}_2 symmetry and drives a single particle band gap (2Δ). Our key prediction is the spontaneous breakdown of a U(1) symmetry, and hence the onset of superfluidity. We stress that the superfluid order parameter [Eq. (7)] is not a ferroelectric; it does not couple linearly to an external electric field. However, it does influence the layer polarization in a measurable way and this opens a unique way to detect the superfluid quantum phase transition. We discuss these details next.

Within the ordered phase $\Delta < \Delta_c$, and at $T = 0$, we appeal to the BCS/Eliashberg gap equation to estimate $\Phi_0(p)$ [for simplicity we, for now, ignore the momentum dependence, such that $\Phi_0(p) = \Phi_0$]. Near the critical point $\Delta \rightarrow \Delta_c$, and to logarithmic accuracy, the gap equation gives $1 = g' \ln(\Lambda'/\sqrt{\Delta^2 + |\Phi_0|^2})$ or $|\Phi_0| = \text{Re}\sqrt{\Delta_c^2 - \Delta^2}$. Here $\Delta_c = \Lambda' e^{-1/g'}$, $g' \sim g$ is a dimensionless combination of the interaction and density of states and $\Lambda' \sim \Lambda$ is a UV cut-off.

The natural, measurable quantity of the system is not Φ_0 , but instead the layer polarization. In the absence of excitonic order, $\Phi_0 = 0$, the polarization is \mathcal{P}_Δ of Eq. (2). Polarization results from the valence electrons belonging predominantly to, say, the bottom layer. Since $\Phi_0 \neq 0$ ultimately corresponds to removing valence electrons (bottom layer) and enhancing conduction electrons (top layer), one expects $\Phi_0 \neq 0$ to reduce the ground state polarization. The polarization in the condensate phase is

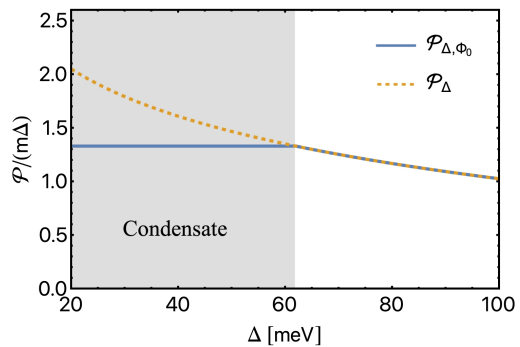


FIG. 4. Dimensionless layer polarization, as a function of band gap parameter Δ , with and without the condensate — corresponding to $\mathcal{P}_{\Delta,\Phi}$ and \mathcal{P}_Δ [Eq. (2)], respectively. Here we use the meanfield expression $|\Phi_0| = \text{Re}\sqrt{\Delta_c^2 - \Delta^2}$, at $T = 0$, with $\Delta_c = 62$ meV corresponding to system parameters $\epsilon_r = 1, d = 1000$ nm. Due to the onset of the condensate Φ , a cusp is seen in reduced layer polarization, $\mathcal{P}_{\Delta,\Phi}/(m\Delta)$, at the critical point Δ_c .

then simply $\mathcal{P}_{\Delta,\Phi_0} = \frac{2m\Delta}{\pi} \ln\left(\Lambda/\sqrt{\Delta^2 + |\Phi_0|^2}\right)$. We see that $\Phi_0 \neq 0$ indeed reduces the layer polarization, with leading correction quadratic in Φ_0 . Further, we appeal to the gap equation solution to arrive a key prediction,

$$\mathcal{P}_{\Delta,\Phi_0} - \mathcal{P}_\Delta = -\frac{m|\Phi_0|^2}{\pi\Delta} \xrightarrow{\Delta \rightarrow \Delta_c^-} -\frac{2m(\Delta_c - \Delta)}{\pi}. \quad (8)$$

This expression shows that there is a linear in Δ (and hence in external electric field E) reduction of the layer polarization in the vicinity of the critical point. We anticipate the polarization being readily measured via quantum capacitance, see e.g. [43–45], which would provide a direct experimental test of the exciton condensation transition.

Finally, we turn to the in-plane real-space structure of the condensate. The intervalley ordering [Eq. (7)] implies that, in real-space, the condensate exhibits a pair density wave pattern, denoting $\tilde{\Phi}_{s,s'}(\mathbf{r}, \mathbf{r}') = \tilde{\Phi}(\mathbf{r}, \mathbf{r}')(d_\mu s_\mu i s_y)_{s,s'}$,

$$\tilde{\Phi}(\mathbf{r}, \mathbf{r}') = \tilde{\Phi}_0(\mathbf{r} - \mathbf{r}') \cos(\mathbf{K} \cdot (\mathbf{r} + \mathbf{r}') + \phi) \quad (9)$$

with $\tilde{\Phi}_0(\mathbf{r} - \mathbf{r}')$ a complex amplitude (derived in the Supplement [41]). Fluctuations of ϕ correspond to gapless sliding modes of the pair density wave. The pair density wave is spatially modulated with a periodicity of three unit cells. In the context of superconductivity, such a density wave pattern has been analysed at length in Ref. [46] and has been linked to higher-order topology in Refs. [47, 48] — we leave the question of higher topology of the mean-field order Eq. (9) for future work.

Discussion — We presented a description for the excitonic bound states in biased BLG, and their subsequent condensation. Owing to biased BLG being a band insulator, we were able to apply two-body techniques. This is contrasted to exciton formation and condensation from

a semi-metallic ground state, whereby many-body techniques are necessary, and resultantly uncontrolled approximations are often required.

We examined suspended biased BLG, with gates $d > d_c \approx 10 - 15$ nm. In this regime/setup, we show that excitons condense for $\Delta < \Delta_c$, Fig. 3(a). This is our primary theoretical finding. For distance to gates $d = 100\text{nm}$ (1000nm) the maximum critical temperature is predicted to be 100K (115K), and is optimised at non-zero bias, Fig. 3(b). Entering the BEC phase, our two-body techniques are no longer quantitatively accurate, however, we are able to establish several qualitative features of the condensate. Experimentally distinguishing between the excitonic condensate/insulator and the band insulator is a challenging task. To this end, we found that the excitons influence the macroscopic dipole moment [c.f. (8)], and

proposed a smoking gun test for exciton condensation – quantum capacitance measurements of the dipole moment as a function of the bias field, which tunes the band insulator to exciton condensate phase transition [c.f. Fig. 4]. We hope to entice direct experimental searches for the excitonic condensate in biased bilayer graphene. Future theoretical work may consider other candidate materials using the two-body approach applied here.

ACKNOWLEDGMENTS

We thank Dmitry Efimkon, Alex Hamilton, Mike Zhitomirsky and Jörg Schmalian for enlightening conversations. We acknowledge funding support from the Australian Research Council Centre of Excellence in Future Low-Energy Electronics Technology (FLEET) (CE170100039).

-
- [1] Y. E. Lozovik and V. I. Yudson, Feasibility of superfluidity of paired spatially separated electrons and holes; a new superconductivity mechanism, *JETP Lett.* (USSR) (Engl. Transl.); (United States).
- [2] M. Pogrebinskii, Mutual drag of carriers in a semiconductor-insulator-semiconductor system, *Soviet Physics-Semiconductors* **11**, 372 (1977).
- [3] J. M. Blatt, K. Böer, and W. Brandt, Bose-einstein condensation of excitons, *Physical Review* **126**, 1691 (1962).
- [4] M. Kellogg, J. Eisenstein, L. Pfeiffer, and K. West, Vanishing hall resistance at high magnetic field in a double-layer two-dimensional electron system, *Physical review letters* **93**, 036801 (2004).
- [5] J.-J. Su and A. MacDonald, How to make a bilayer exciton condensate flow, *Nature Physics* **4**, 799 (2008).
- [6] R. Wang, O. Erten, B. Wang, and D. Y. Xing, Prediction of a topological $p + ip$ excitonic insulator with parity anomaly, *Nature Communications* **10**, 210 (2019).
- [7] D. Varsano, M. Palummo, E. Molinari, and M. Rontani, A monolayer transition-metal dichalcogenide as a topological excitonic insulator, *Nature Nanotechnology* **15**, 367 (2020).
- [8] E. Peretto and G. Stefanucci, Floquet topological phase of nondriven p -wave nonequilibrium excitonic insulators, *Phys. Rev. Lett.* **125**, 106401 (2020).
- [9] Z. Sun and A. J. Millis, Topological charge pumping in excitonic insulators, *Phys. Rev. Lett.* **126**, 027601 (2021).
- [10] Z.-R. Liu, L.-H. Hu, C.-Z. Chen, B. Zhou, and D.-H. Xu, Topological excitonic corner states and nodal phase in bilayer quantum spin hall insulators, *Phys. Rev. B* **103**, L201115 (2021).
- [11] H. D. Scammell, J. Ingham, T. Li, and O. P. Sushkov, Chiral excitonic order, quantum anomalous hall effect, and superconductivity from twofold van hove singularities in kagome metals (2022), [arXiv:2201.02643 \[cond-mat.supr-con\]](https://arxiv.org/abs/2201.02643).
- [12] L. V. Keldysh and Y. V. Kopaev, Possible instability of the semimetallic state against coulomb interaction, *Fiz. Tverd. Tela.*, **6**, 2791 (1964) [*Sov. Phys. Solid State* **6**, 2219 (1965)] (1964).
- [13] D. Jérôme, T. M. Rice, and W. Kohn, Excitonic insulator, *Phys. Rev.* **158**, 462 (1967).
- [14] B. Halperin and T. Rice, The excitonic state at the semiconductor-semimetal transition (Academic Press, 1968) pp. 115–192.
- [15] R. Nandkishore and L. Levitov, Dynamical screening and excitonic instability in bilayer graphene, *Phys. Rev. Lett.* **104**, 156803 (2010).
- [16] K. W. Song, Y.-C. Liang, and S. Haas, Excitonic instabilities and insulating states in bilayer graphene, *Phys. Rev. B* **86**, 205418 (2012).
- [17] V. Apinyan and T. K. Kopeć, Excitonic gap formation and condensation in the bilayer graphene structure, *Physica Scripta* **91**, 095801 (2016).
- [18] R. S. Akzyanov, A. O. Sboychakov, A. V. Rozhkov, A. L. Rakhmanov, and F. Nori, aa -stacked bilayer graphene in an applied electric field: Tunable antiferromagnetism and coexisting exciton order parameter, *Phys. Rev. B* **90**, 155415 (2014).
- [19] V. Apinyan and T. K. Kopeć, Antiferromagnetic ordering and excitonic pairing in aa -stacked bilayer graphene, *Phys. Rev. B* **104**, 075426 (2021).
- [20] H. Min, R. Bistritzer, J.-J. Su, and A. H. MacDonald, Room-temperature superfluidity in graphene bilayers, *Phys. Rev. B* **78**, 121401 (2008).
- [21] Y. E. Lozovik and A. A. Sokolik, Electron-hole pair condensation in a graphene bilayer, *JETP Letters* **87**, 55 (2008).
- [22] C.-H. Zhang and Y. N. Joglekar, Excitonic condensation of massless fermions in graphene bilayers, *Phys. Rev. B* **77**, 233405 (2008).
- [23] M. Y. Kharitonov and K. B. Efetov, Electron screening and excitonic condensation in double-layer graphene systems, *Phys. Rev. B* **78**, 241401 (2008).
- [24] M. Y. Kharitonov and K. B. Efetov, Excitonic condensation in a double-layer graphene system, *Semiconductor Science and Technology* **25**, 034004 (2010).
- [25] A. Perali, D. Neilson, and A. R. Hamilton, High-temperature superfluidity in double-bilayer graphene, *Phys. Rev. Lett.* **110**, 146803 (2013).
- [26] J.-J. Su and A. H. MacDonald, Spatially indirect exciton condensate phases in double bilayer graphene, *Phys. Rev.*

- B **95**, 045416 (2017).
- [27] D. K. Efimkin, G. W. Burg, E. Tutuc, and A. H. MacDonald, Tunneling and fluctuating electron-hole cooper pairs in double bilayer graphene, *Phys. Rev. B* **101**, 035413 (2020).
- [28] S. Conti, A. Perali, F. M. Peeters, and D. Neilson, Multi-component screening and superfluidity in gapped electron-hole double bilayer graphene with realistic bands, *Phys. Rev. B* **99**, 144517 (2019).
- [29] G. W. Burg, N. Prasad, K. Kim, T. Taniguchi, K. Watanabe, A. H. MacDonald, L. F. Register, and E. Tutuc, Strongly enhanced tunneling at total charge neutrality in double-bilayer graphene-wse₂ heterostructures, *Phys. Rev. Lett.* **120**, 177702 (2018).
- [30] L. Du, X. Li, W. Lou, G. Sullivan, K. Chang, J. Kono, and R.-R. Du, Evidence for a topological excitonic insulator in inas/gasb bilayers, *Nature Communications* **8**, 1971 (2017).
- [31] X. Liu, K. Watanabe, T. Taniguchi, B. I. Halperin, and P. Kim, Quantum hall drag of exciton condensate in graphene, *Nature Physics* **13**, 746 (2017).
- [32] J. I. A. Li, T. Taniguchi, K. Watanabe, J. Hone, and C. R. Dean, Excitonic superfluid phase in double bilayer graphene, *Nature Physics* **13**, 751 (2017).
- [33] J. I. A. Li, Q. Shi, Y. Zeng, K. Watanabe, T. Taniguchi, J. Hone, and C. R. Dean, Pairing states of composite fermions in double-layer graphene, *Nature Physics* **15**, 898 (2019).
- [34] M. Kellogg, J. P. Eisenstein, L. N. Pfeiffer, and K. W. West, Vanishing hall resistance at high magnetic field in a double-layer two-dimensional electron system, *Phys. Rev. Lett.* **93**, 036801 (2004).
- [35] E. Tutuc, M. Shayegan, and D. A. Huse, Counterflow measurements in strongly correlated gas hole bilayers: Evidence for electron-hole pairing, *Phys. Rev. Lett.* **93**, 036802 (2004).
- [36] R. D. Wiersma, J. G. S. Lok, S. Kraus, W. Dietsche, K. von Klitzing, D. Schuh, M. Bichler, H.-P. Tranitz, and W. Wegscheider, Activated transport in the separate layers that form the $\nu_T = 1$ exciton condensate, *Phys. Rev. Lett.* **93**, 266805 (2004).
- [37] E. McCann and M. Koshino, The electronic properties of bilayer graphene, *Reports on Progress in Physics* **76**, 056503 (2013).
- [38] E. McCann and V. I. Fal'ko, Landau-level degeneracy and quantum hall effect in a graphite bilayer, *Phys. Rev. Lett.* **96**, 086805 (2006).
- [39] Y. Zhang, T.-T. Tang, C. Girit, Z. Hao, M. C. Martin, A. Zettl, M. F. Crommie, Y. R. Shen, and F. Wang, Direct observation of a widely tunable bandgap in bilayer graphene, *Nature* **459**, 820 (2009).
- [40] H. D. Scammell and O. P. Sushkov, *Dynamical screening and excitonic bound states in biased bilayer graphene* (2022).
- [41] See Supplemental Material for more details on the polarization operator, the form factors, the critical temperature scaling, and the real-space order parameter.
- [42] V. Berestetskii, E. Lifshitz, and L. Pitaevskii, *Quantum Electrodynamics: Volume 4*, Course of theoretical physics (Elsevier Science, 1982).
- [43] M. J. Yang, C. H. Yang, B. R. Bennett, and B. V. Shanabrook, Evidence of a hybridization gap in "semimetallic" InAs/GaSb systems, *Phys. Rev. Lett.* **78**, 4613 (1997).
- [44] L. Du, X. Li, W. Lou, G. Sullivan, K. Chang, J. Kono, and R.-R. Du, Evidence for a topological excitonic insulator in inas/gasb bilayers, *Nature communications* **8**, 1 (2017).
- [45] S. Saberi-Pouya, S. Conti, A. Perali, A. F. Croxall, A. R. Hamilton, F. M. Peeters, and D. Neilson, Experimental conditions for the observation of electron-hole superfluidity in gas heterostructures, *Physical Review B* **101**, 140501 (2020).
- [46] B. Roy and I. F. Herbut, Unconventional superconductivity on honeycomb lattice: Theory of kekule order parameter, *Phys. Rev. B* **82**, 035429 (2010).
- [47] T. Li, J. Ingham, and H. D. Scammell, Artificial graphene: Unconventional superconductivity in a honeycomb superlattice, *Phys. Rev. Research* **2**, 043155 (2020).
- [48] T. Li, M. Geier, J. Ingham, and H. D. Scammell, Higher-order topological superconductivity from repulsive interactions in kagome and honeycomb systems, *2D Materials* **9**, 015031 (2021).

SUPPLEMENTAL MATERIAL

I. HAMILTONIAN AND WAVEFUNCTIONS

The Hamiltonian and wavefunctions are (in zero field)

$$\begin{aligned}
 H_\tau &= -\frac{(\tau p_x \mp i p_y)^2}{2m} \sigma_\pm + \Delta \sigma_z \\
 |\psi_{\mathbf{p},\tau}^{(+)}\rangle &= \frac{1}{\sqrt{\frac{(\epsilon_{\mathbf{p}} - \Delta)^2}{p^4/(4m^2)} + 1}} \begin{pmatrix} -1 \\ \frac{\epsilon_{\mathbf{p}} - \Delta}{p^2/(2m)} e^{2i\tau\theta_{\mathbf{p}}} \end{pmatrix}, \\
 |\psi_{\mathbf{p},\tau}^{(-)}\rangle &= \mathcal{P} |\psi_{\mathbf{p},\tau}^{(+)}\rangle = \frac{1}{\sqrt{\frac{(\epsilon_{\mathbf{p}} - \Delta)^2}{p^4/(4m^2)} + 1}} \begin{pmatrix} \frac{\epsilon_{\mathbf{p}} - \Delta}{p^2/(2m)} e^{-2i\tau\theta_{\mathbf{p}}} \\ 1 \end{pmatrix}, \\
 \mathcal{P} &= i\sigma_y \mathcal{C}.
 \end{aligned} \tag{S1}$$

The operator \mathcal{P} generates the particle-hole transformation, which is an (anti)symmetry of this Hamiltonian. Defining ψ_- in this way correctly generates the phase/winding factors.

II. POLARIZATION OPERATOR

The expression for the polarization generically takes the form,

$$\Pi(\mathbf{q}, i\xi, T) = 4 \sum_{\mu, \nu = \pm} \int \frac{d^2 p}{(2\pi)^2} \frac{(f_{\epsilon_{\mathbf{p}}^\mu} - f_{\epsilon_{\mathbf{p}+\mathbf{q}}^\nu})}{i\xi + \epsilon_{\mathbf{p}}^\mu - \epsilon_{\mathbf{p}+\mathbf{q}}^\nu} F_{\mathbf{p}, \mathbf{p}+\mathbf{q}}^{\mu\nu}. \tag{S2}$$

Here the form factors are $F_{\mathbf{p}, \mathbf{p}+\mathbf{q}}^{\mu\nu} = |\langle \psi_{\mathbf{p}+\mathbf{q}, \tau}^{(\mu)} | \psi_{\mathbf{p}, \tau}^{(\nu)} \rangle|^2$, with $\mu, \nu = \pm$. Using that $-\epsilon_{\mathbf{p}}^- = \epsilon_{\mathbf{p}}^+ \equiv \epsilon_{\mathbf{p}}$ and $F_{\mathbf{p}, \mathbf{p}+\mathbf{q}}^{--} = F_{\mathbf{p}, \mathbf{p}+\mathbf{q}}^{++}$, $F_{\mathbf{p}, \mathbf{p}+\mathbf{q}}^{-+} = F_{\mathbf{p}, \mathbf{p}+\mathbf{q}}^{+-}$, we get

$$\Pi(\mathbf{q}, i\xi, T) = 8 \int \frac{d^2 p}{(2\pi)^2} \left[\frac{(\epsilon_{\mathbf{p}} - \epsilon_{\mathbf{p}+\mathbf{q}})(f_{\epsilon_{\mathbf{p}}} - f_{\epsilon_{\mathbf{p}+\mathbf{q}}})}{\xi^2 + (\epsilon_{\mathbf{p}} - \epsilon_{\mathbf{p}+\mathbf{q}})^2} F_{\mathbf{p}, \mathbf{p}+\mathbf{q}}^{++} + \frac{(\epsilon_{\mathbf{p}} + \epsilon_{\mathbf{p}+\mathbf{q}})(f_{\epsilon_{\mathbf{p}}} + f_{\epsilon_{\mathbf{p}+\mathbf{q}}} - 1)}{\xi^2 + (\epsilon_{\mathbf{p}} + \epsilon_{\mathbf{p}+\mathbf{q}})^2} F_{\mathbf{p}, \mathbf{p}+\mathbf{q}}^{+-} \right]. \tag{S3}$$

III. VERTEX FORM FACTORS

The Coulomb interaction is taken to be

$$H_{int} = \sum_{\mathbf{p}_1, \mathbf{p}_2, \mathbf{p}_3} \sum_{\tau, \tau'} V(\mathbf{p}_2 - \mathbf{p}_1) \Psi_{\mathbf{p}_1, \tau}^\dagger \Psi_{\mathbf{p}_2, \tau'}^\dagger \Psi_{\mathbf{p}_3, \tau'} \Psi_{\mathbf{p}_1 + \mathbf{p}_2 - \mathbf{p}_3, \tau}, \tag{S4}$$

which neglects valley-exchange. We transform to band basis,

$$\Psi_{\mathbf{p}, \tau} = \mathcal{U}_{\mathbf{p}, \tau} \begin{pmatrix} c_{\mathbf{p}, \tau} \\ v_{\mathbf{p}, \tau} \end{pmatrix}, \quad \mathcal{U}_{\mathbf{p}, \tau} = (|\psi_{\mathbf{p}, \tau}^{(+)}\rangle, |\psi_{\mathbf{p}, \tau}^{(-)}\rangle),$$

with $c_{\mathbf{p}, \tau}$ and $v_{\mathbf{p}, \tau}$ the destruction operators for conduction and valence electrons. Restricting consideration to the exciton channel, denoted H_{int}^X , the interaction becomes,

$$H_{int}^X = \sum_{\mathbf{p}_1, \mathbf{p}_2} \sum_{\tau, \tau'} V(\mathbf{p}_2 - \mathbf{p}_1) c_{\mathbf{p}_1, \tau}^\dagger c_{\mathbf{p}_2, \tau} v_{\mathbf{p}_2, \tau'}^\dagger v_{\mathbf{p}_1, \tau'} \langle \psi_{\mathbf{p}_2, \tau'}^{(-)} | \psi_{\mathbf{p}_1, \tau'}^{(-)} \rangle \langle \psi_{\mathbf{p}_1, \tau}^{(+)} | \psi_{\mathbf{p}_2, \tau}^{(+)} \rangle. \tag{S5}$$

In the main text we denote the form factor $Z_{\mathbf{p}_1, \mathbf{p}_2}^{\tau', \tau} = \langle \psi_{\mathbf{p}_2, \tau'}^{(-)} | \psi_{\mathbf{p}_1, \tau'}^{(-)} \rangle \langle \psi_{\mathbf{p}_1, \tau}^{(+)} | \psi_{\mathbf{p}_2, \tau}^{(+)} \rangle$.

IV. CRITICAL TEMPERATURE SCALING

Setting $E = 0$, the $T = 0$ the Lippmann-Schwinger equation gives the condition for Δ_c

$$2\sqrt{\frac{p^4}{4m^2} + \Delta_c^2}\Psi_{\mathbf{p}} = \int \frac{d^2p'}{(2\pi)^2} V_{\mathbf{p},\mathbf{p}'}^0 \Psi_{\mathbf{p}'}. \quad (\text{S6})$$

At $T > 0$, the condition $E = 0$ requires $\Delta < \Delta_c$, and is given by

$$2\sqrt{\frac{p^4}{4m^2} + \Delta^2}\Psi_{\mathbf{p}} = \int \frac{d^2p'}{(2\pi)^2} \left[V_{\mathbf{p},\mathbf{p}'}^0 + \delta V_{\mathbf{p},\mathbf{p}'} e^{-\frac{\Delta}{T_c}} \right] \Psi_{\mathbf{p}'}. \quad (\text{S7})$$

Using that the characteristic momentum is $p = \sqrt{2m\Delta}$, we combine these two equations as

$$\begin{aligned} \Delta_c &= \nu_0, \\ \Delta &= \left(\nu_0 - \nu_1 e^{-\frac{\Delta}{T_c}} \right), \\ (\Delta_c - \Delta) &= \nu_1 e^{-\frac{\Delta}{T_c}}, \rightarrow T_c = \Delta / \ln \left(\frac{\nu_1}{\Delta_c - \Delta} \right). \end{aligned} \quad (\text{S8})$$

V. REAL-SPACE ORDER PARAMETER

In this appendix we derive the effective lattice model for the dominant excitonic order parameter. Introducing the real-space creation operators for the conduction and valence bands via,

$$\begin{aligned} c_{\mathbf{p},\tau,s}^\dagger &= \sum_{\mathbf{r}} \phi_{\mathbf{p},\tau}^{(+)}(\mathbf{r}) \tilde{c}_{\mathbf{r},s}^\dagger, \\ v_{\mathbf{p},\tau,s}^\dagger &= \sum_{\mathbf{r}} \phi_{\mathbf{p},\tau}^{(-)}(\mathbf{r}) \tilde{v}_{\mathbf{r},s}^\dagger. \end{aligned} \quad (\text{S9})$$

With \mathbf{r} spanning the real-space lattice sites, and comprising two sublattices, $\sigma = A_1, B_2$, and $\{a(\mathbf{r} \in A) = 1, a(\mathbf{r} \in B) = 0\}$ and $\{b(\mathbf{r} \in A) = 0, b(\mathbf{r} \in B) = 1\}$. Here,

$$\begin{aligned} \phi_{\mathbf{p},\tau}^{(+)}(\mathbf{r}) &= e^{i(\mathbf{p}+\tau\mathbf{K})} \left(\alpha_{\tau,\mathbf{k}}^{(+)} a(\mathbf{r}) + \beta_{\tau,\mathbf{k}}^{(+)} b(\mathbf{r}) \right), \\ \phi_{\mathbf{p},\tau}^{(-)}(\mathbf{r}) &= e^{i(\mathbf{p}+\tau\mathbf{K})} \left(\alpha_{\tau,\mathbf{k}}^{(-)} a(\mathbf{r}) + \beta_{\tau,\mathbf{k}}^{(-)} b(\mathbf{r}) \right), \end{aligned} \quad (\text{S10})$$

with definitions,

$$\begin{aligned} \alpha_{\tau,\mathbf{p}}^{(+)} &= -\cos \gamma_{\mathbf{p}} = \frac{-1}{\sqrt{\frac{(\varepsilon_{\mathbf{p}} - \Delta)^2}{p^4/(4m^2)} + 1}}, \\ \beta_{\tau,\mathbf{p}}^{(+)} &= \sin \gamma_{\mathbf{p}} e^{2i\tau\theta_{\mathbf{p}}} = \frac{\varepsilon_{\mathbf{p}} - \Delta}{p^2/(2m)} \frac{e^{2i\tau\theta_{\mathbf{p}}}}{\sqrt{\frac{(\varepsilon_{\mathbf{p}} - \Delta)^2}{p^4/(4m^2)} + 1}}, \\ \alpha_{\tau,\mathbf{p}}^{(-)} &= \sin \gamma_{\mathbf{p}} e^{-2i\tau\theta_{\mathbf{p}}} = \frac{\varepsilon_{\mathbf{p}} - \Delta}{p^2/(2m)} \frac{e^{-2i\tau\theta_{\mathbf{p}}}}{\sqrt{\frac{(\varepsilon_{\mathbf{p}} - \Delta)^2}{p^4/(4m^2)} + 1}}, \\ \beta_{\tau,\mathbf{p}}^{(-)} &= \cos \gamma_{\mathbf{p}} = \frac{1}{\sqrt{\frac{(\varepsilon_{\mathbf{p}} - \Delta)^2}{p^4/(4m^2)} + 1}}. \end{aligned} \quad (\text{S11})$$

The mean-field Hamiltonian becomes,

$$H_{\Phi} = \sum_{\mathbf{p},\tau,\tau',s,s'} c_{\mathbf{p},\tau,s}^\dagger \Phi_{\tau,\tau',s,s'} v_{\mathbf{p},\tau',s'} = \sum_{\mathbf{p},\tau,\tau',s,s'} \sum_{\mathbf{r},\mathbf{r}'} \phi_{\mathbf{p},\tau}^{(+)}(\mathbf{r}) (\phi_{\mathbf{p},\tau'}^{(-)})^*(\mathbf{r}') \Phi_{\tau,\tau',s,s'} \tilde{c}_{\mathbf{r},s}^\dagger \tilde{v}_{\mathbf{r}',s'} + \text{h.c.} \quad (\text{S12})$$

We consider intervalley pairing in the s -wave channel and with arbitrary spin ordering (singlet or triplet). There is both a symmetric and an anti-symmetric combination of the valleys,

$$\Phi(p)_{\tau,\tau',s,s'} = \begin{cases} \Phi_0(p)(\tau_x)_{\tau,\tau'}(d_\mu s_\mu)_{s,s'} \\ \Phi_0(p)(i\tau_y)_{\tau,\tau'}(d_\mu s_\mu)_{s,s'}. \end{cases} \quad (\text{S13})$$

In fact, there is a $U(1)$ rotational symmetry that connects these distinct valley structures – we more compactly write

$$\Phi(p)_{\tau,\tau',s,s'} = \Phi_0(p)(\tau_x)_{\tau,\tau'} e^{i\frac{(\tau-\tau')}{2}\phi} \phi(d_\mu s_\mu)_{s,s'} \quad (\text{S14})$$

Let us consider the case that $\mathbf{r} \in A$ and $\mathbf{r}' \in B$,

$$\begin{aligned} H_\Phi^{AB} &= \sum_{\mathbf{p},\tau,s,s'} \sum_{\mathbf{r} \in A, \mathbf{r}' \in B} \left(e^{i(\mathbf{p}+\tau\mathbf{K})\cdot\mathbf{r}} \alpha_{\tau,\mathbf{p}}^{(+)} a(\mathbf{r}) \right) \left(e^{-i(\mathbf{p}-\tau\mathbf{K})\cdot\mathbf{r}'} \beta_{-\tau,\mathbf{p}}^{(-)} b(\mathbf{r}') \right) \Phi_0(p) e^{i\tau\phi} \tilde{c}_{\mathbf{r},s}^\dagger \tilde{v}_{\mathbf{r}',s'}(d_\mu s_\mu)_{s,s'} + \text{h.c.} \\ &= \sum_{\mathbf{p},\tau,s,s'} \sum_{\mathbf{r} \in A, \mathbf{r}' \in B} \left[e^{i\mathbf{p}\cdot(\mathbf{r}-\mathbf{r}')} e^{i\tau\mathbf{K}\cdot(\mathbf{r}+\mathbf{r}')} \alpha_{\tau,\mathbf{p}}^{(+)} \beta_{-\tau,\mathbf{p}}^{(-)} \Phi_0(p) e^{i\tau\phi} \right] \tilde{c}_{\mathbf{r},s}^\dagger \tilde{v}_{\mathbf{r}',s'}(d_\mu s_\mu)_{s,s'} + \text{h.c.} , \\ &= \sum_{\mathbf{r} \in A, \mathbf{r}' \in B} \sum_{\mathbf{p}} \left[2e^{i\mathbf{p}\cdot(\mathbf{r}-\mathbf{r}')} (-\cos^2 \gamma_{\mathbf{p}}) \Phi_0(p) \right] [\cos(\mathbf{K} \cdot (\mathbf{r} + \mathbf{r}') + \phi)] \sum_{s,s'} \tilde{c}_{\mathbf{r},s}^\dagger \tilde{v}_{\mathbf{r}',s'}(d_\mu s_\mu)_{s,s'} + \text{h.c.} , \\ &= \sum_{\mathbf{r} \in A, \mathbf{r}' \in B} \Gamma^{AB}(\mathbf{r} - \mathbf{r}') [\cos(\mathbf{K} \cdot (\mathbf{r} + \mathbf{r}') + \phi)] \sum_{s,s'} \tilde{c}_{\mathbf{r},s}^\dagger \tilde{v}_{\mathbf{r}',s'}(d_\mu s_\mu)_{s,s'} + \text{h.c.} . \end{aligned} \quad (\text{S15})$$

We have defined the function,

$$\Gamma^{AB}(\mathbf{r} - \mathbf{r}') \equiv \sum_{\mathbf{p}} \left[2e^{i\mathbf{p}\cdot(\mathbf{r}-\mathbf{r}')} (-\cos^2 \gamma_{\mathbf{p}}) \Phi_0(p) \right], \quad (\text{S16})$$

which determines the real-space amplitude and can be directly evaluated numerically.

Performing the same procedure for all combinations of \mathbf{r}, \mathbf{r}' in $\{A_1, B_2\}$, we arrive at the expression,

$$H_\Phi = \sum_{\mathbf{r}, \mathbf{r}'} \Gamma(\mathbf{r} - \mathbf{r}') [\cos(\mathbf{K} \cdot (\mathbf{r} + \mathbf{r}') + \phi)] \sum_{s,s'} \tilde{c}_{\mathbf{r},s}^\dagger \tilde{v}_{\mathbf{r}',s'}(d_\mu s_\mu)_{s,s'} + \text{h.c.}, \quad (\text{S17})$$

with amplitude function,

$$\Gamma(\mathbf{r} - \mathbf{r}') = \begin{cases} \Gamma^{AA}(\mathbf{r} - \mathbf{r}') = \sum_{\mathbf{p}} \left[2e^{i\mathbf{p}\cdot(\mathbf{r}-\mathbf{r}')} (-\cos \gamma_{\mathbf{p}} \sin \gamma_{\mathbf{p}} e^{\pm 2i\tau\theta_{\mathbf{p}}}) \Phi_0(p) \right], \text{ for } \{\mathbf{r} \in A_1, \mathbf{r}' \in A_1\} \\ \Gamma^{BB}(\mathbf{r} - \mathbf{r}') = \sum_{\mathbf{p}} \left[2e^{i\mathbf{p}\cdot(\mathbf{r}-\mathbf{r}')} (\cos \gamma_{\mathbf{p}} \sin \gamma_{\mathbf{p}} e^{\pm 2i\tau\theta_{\mathbf{p}}}) \Phi_0(p) \right], \text{ for } \{\mathbf{r} \in B_2, \mathbf{r}' \in B_2\} \\ \Gamma^{AB}(\mathbf{r} - \mathbf{r}') = \sum_{\mathbf{p}} \left[2e^{i\mathbf{p}\cdot(\mathbf{r}-\mathbf{r}')} (-\cos^2 \gamma_{\mathbf{p}}) \Phi_0(p) \right], \text{ for } \{\mathbf{r} \in A_1, \mathbf{r}' \in B_2\} \\ \Gamma^{BA}(\mathbf{r} - \mathbf{r}') = \sum_{\mathbf{p}} \left[2e^{i\mathbf{p}\cdot(\mathbf{r}-\mathbf{r}')} (\sin^2 \gamma_{\mathbf{p}} e^{\pm 4i\theta_{\mathbf{p}}}) \Phi_0(p) \right], \text{ for } \{\mathbf{r} \in B_2, \mathbf{r}' \in A_1\}. \end{cases} \quad (\text{S18})$$